An Optimum Coaxial Rotor System for Axial Flight

J. Gordon Leishman*
Minta Martin Professor of Engineering

Shreyas Ananthan
Assistant Research Scientist

Department of Aerospace Engineering
Glenn L. Martin Institute of Technology
University of Maryland, College Park, MD

The concept of a coaxial rotor system that is optimized for most efficient hovering and/or axial flight performance is discussed. A blade-element momentum theory (BEMT) for a coaxial rotor system was developed and implemented numerically. The BEMT was found to agree well with performance measurements (thrust and power) made on coaxial helicopter rotors and on single and contrarotating propellers. Good correlation was also found with performance and spanwise loadings predicted by a free-vortex wake method, thereby helping to validate the assumptions made with the BEMT and better assess its overall predictive capabilities at the blade-element level. Furthermore, the BEMT was shown to give better performance predictions than using the simple momentum theory. The BEMT predicts that the optimum or "ideal" performing condition for a coaxial rotor in axial flight occurs when both the upper and lower rotors operate at uniform disk loadings at a torque-balanced condition. This operating condition corresponds to linear distributions of thrust over both the upper and lower rotors. The ideal case also corresponds to uniform inflow over the upper rotor, but a double-valued variation of uniform inflow over the lower rotor. The optimum blade twist for minimum induced losses on the lower rotor is of double hyperbolic form, with the break point in the twist being at the radial location where the outer edge of the wake boundary from the upper rotor is assumed to impinge on the lower rotor. The results also show that at the most efficient torque-balanced operating condition, the upper and lower rotors of the coaxial operate at different mean lift coefficients, so that an optimum performing coaxial rotor in hover or axial flight will require different blade planforms (i.e., solidities) on both rotors to minimize profile losses.

Nomenclature

A	rotor disk area (for one rotor), m^2
A_c	contracted slipstream wake area, m^2
a	nondimensional radial contraction of upper wake
C_d	drag coefficient
C_{d_0}	minimum or zero-lift profile drag coefficient
C_l	lift coefficient
C_{l_α}	lift-curve-slope (two-dimensional), rad^{-1}
C_P	rotor power coefficient, $= P/\rho A\Omega^3 R^3$
C_Q	rotor torque coefficient, $= Q/\rho A\Omega^2 R^3$
C_T	rotor thrust coefficient, $= T/\rho A\Omega^2 R^2$
C_W	weight coefficient, $= W/\rho A\Omega^2 R^2$
c	blade chord, m
D	propeller diameter, m
F	Prandtl tip loss function
f	exponent in Prandtl tip loss function
FM	rotor system figure of merit
J	propeller advance ratio, V_∞/nD
$\dot{m}$	mass flow rate, $kg\,ms^{-1}$
N_b	number of blades (for one rotor)
n	revolutions per second
P	rotor power, kW
Q	rotor torque, Nm
R	radius of blade, m
r	nondimensional radial span position
T	rotor thrust, N
V_∞	axial flight velocity, ms^{-1}
v	induced velocity, ms^{-1}
W	vehicle weight, N
y	radial coordinate, m
η	propulsive efficiency
θ	blade pitch, rad
κ	rotor-induced power factor (single rotor)
κ_{int}	induced power interference factor for a coaxial
λ	nondimensional average inflow velocity, $v/\Omega R$
λ_∞	nondimensional axial velocity, $V_\infty/\Omega R$
ρ	air density, $kg\,m^{-3}$
σ	rotor solidity, $N_b c/\pi R$
ϕ	inflow angle, rad
Ω	rotational speed of the rotor, $rad\,s^{-1}$

Subscripts and Superscripts

l	refers to lower (or rear) rotor
u	refers to upper (or front) rotor

Introduction

There has been a recent surge of renewed interest in contrarotating coaxial rotor systems for use with helicopters, tiltrotors, and micro air

*Corresponding author; email: leishman@umd.edu.
Manuscript received August 2007; accepted August 2008.

vehicles (MAVs); see, for example, Refs. 1–3. When used on a helicopter, a coaxial rotor system has two important advantages: (1) It eliminates the need for a separate antitorque system and (2) overall rotor diameter can be reduced relative to that of a single rotor to produce comparable net thrust with the same (or similar) disk and blade loadings. Both of these advantages make the resulting aircraft significantly smaller, although not necessarily lighter or more efficient. There are further advantages of a coaxial rotor for an advancing blade concept helicopter using semirigid blades (Ref. 1), which can potentially achieve much higher forward speeds compared to a conventional helicopter. A coaxial proprotor may also have certain advantages when used on a tiltrotor (Ref. 2), including the possibility of more robust operating margins (Ref. 4).

However, a distinct disadvantage with a coaxial is that the flows between the two rotors interact, and there is a reciprocal effect of one rotor upon the other. In particular, the lower rotor operates in the wake slipstream of the upper rotor, so giving a loss of net aerodynamic efficiency from increased induced losses, and also from viscous losses from blade–wake interactions. High interrotor plane spacing has been found desirable to reduce these losses. However, the need for high rotor spacing produces a significant disadvantage when a coaxial rotor is used on a helicopter because of the parasitic drag from the exposed shaft and blade pitch controls between the two rotors. This can reduce substantially the forward flight performance. Nevertheless, by taking into account the interference losses of one rotor upon the other suggests that, at least as a hovering platform, a coaxial rotor system can be just as efficient as when using a conventional single main rotor and tail rotor system, especially if the blade shapes of the coaxial can be carefully optimized to minimize induced, profile, and interference losses.

Coleman (Ref. 5) has summarized previous research on coaxial rotor systems and gives a comprehensive list of relevant citations on performance issues, measured wake flow characteristics, and possible methods of performance analysis. More recent experimental work on coaxial rotors has been conducted by McAlister et al. (Refs. 6, 7), confirming the difficulties in quantifying coaxial rotor performance and measuring the nature of the interfering rotor flow fields. There has also been some theoretical analyses of coaxial rotor performance (albeit relatively limited), mainly by Andrew (Ref. 8), Saito and Azuma (Ref. 9), Zimmer (Ref. 10), Valkov (Ref. 11) and a few others; again see Coleman (Ref. 5) for a summary of most of the early work. Studies of coaxial rotors using computational fluid dynamics (CFD) is much more recent (Refs. 12, 13). However, none of these investigations (experimental or CFD) have led to clear design guidelines that can be used to help maximize (or otherwise optimize) the aerodynamic performance of a coaxial rotor system to achieve a required level of performance, and more often than not the design process (especially for MAVs) seems to proceed on an almost ad hoc basis.

Clearly, the general problem of designing a high-performing coaxial rotor is indeed complicated. Besides the primary aerodynamic effects that are associated with rotor-on-rotor interference, any method must represent several interdependent aerodynamic influences. These include the effects of blade twist, planform shapes, airfoil sections, and the need to predict nonideal induced and viscous losses that come from the influence of the wake generated by the upper rotor on the performance of the lower rotor. The effects of the lower rotor on the upper rotor also needs to be considered, in that the load sharing between the rotors must affect the net system performance. Therefore, the main goal of the present work was to develop a rational modeling basis to start the process of aerodynamically optimizing a coaxial rotor system to achieve a given level of performance. This process may have several significant design constraints, including rotor plane separation, overall size, maximum allowable blade twist, etc.

To this end, a blade-element momentum theory (BEMT) analysis was developed for an open (i.e., unducted) coaxial rotor system operating in hover and in axial flight. The effort has application to several concurrent vehicle design problems, including coaxial helicopter rotors, tiltrotors with coaxial proprotors, and various types of MAVs. Validation of the BEMT was conducted against measurements for a hovering coaxial helicopter rotor and also for single and coaxial contrarotating propellers operating in axial flight. The main objective was to use the BEMT to help determine a baseline optimum coaxial rotor for further, more detailed analysis, by vortex methods and by CFD. This effort should then lead to a better understanding of the design trades necessary to achieve the maximum efficiency of a coaxial helicopter rotor in hover, or a proprotor when operated in axial flight. An interesting outcome of the present analysis shows that a coaxial rotor system properly optimized for maximum efficiency will need different blade twist distributions and planform shapes on both the upper and lower rotors.

BEMT for a Coaxial Rotor

The BEMT is a form of hybrid analysis method that was first developed in analytical form for propellers by Weick (Ref. 14). This now classic approach contains the essence of Froude's original differential theory for single propellers in axial motion (Ref. 15), but see also Drzewiecki (Ref. 16) and Tokaty (Ref. 17). Gessow (Ref. 18) proposed a variation of the BEMT for the analysis of single helicopter rotors, which is summarized by Gessow and Myers (Ref. 19), and the numerical approach is outlined by Leishman (Ref. 20). The BEMT has become a standard method of helicopter rotor analysis in axial flight, although it has not been previously formalized for a coaxial rotor system except for one attempt by Valkov (Ref. 11). A major advantage of the BEMT is that it is a parsimonious model, built on solid physical principles, which is relatively free of empirical parameters other than airfoil section data.

The BEMT basically amalgamates the blade-element (i.e., section-by-section) and simple momentum theory (SMT) approaches. The principles of the BEMT involve the use of the three conservation laws (i.e., mass, momentum, and energy) applied to successive annuli of the rotor disk and the invocation of the formal equivalence between the circulation and momentum theories of lift generation. There is an assumption that successive blade elements and rotor annuli (on any one rotor) have no mutual effects on each other, i.e., a two-dimensional assumption, an issue first explored experimentally by Lock et al. (Ref. 21). Classic Prandtl "tip loss" effects (Ref. 20) can be included into the BEMT, thereby approximately accounting for the three-dimensional induced flow effects at the blade tips.

Several of the assumptions needed with the SMT for a rotor are removed when using the BEMT, and so its predictive capabilities potentially become much more powerful. This includes the ability to calculate the distributions of aerodynamic loads over the blades, provide estimates of nonideal induced losses and tip losses, and also to estimate the effects of rotor-on-rotor interference, the latter which do not need to be specified a priori as is required with the SMT (Refs. 22, 23). Furthermore, the magnitudes of these various losses are not scalable (which is assumed in the simple theory) and they change with rotor operating state, i.e., with net system thrust and with the thrust sharing between the upper and lower rotors. The BEMT integrates to the SMT in the limiting case of uniformly distributed disk loading (or uniform inflow for a single rotor) without tip losses.

The flow model used here for the coaxial rotor system is shown in Fig. 1. It is assumed that the lower rotor operates partly in the fully developed slipstream of the upper rotor (i.e., in the vena contracta), where there is a maximum change in slipstream velocity before the wake flow enters the plane of the lower rotor. The wake contraction can be assumed based on ideal fluid flow behavior, or otherwise specified through some empirical observation of the resulting wake developments. In practice,

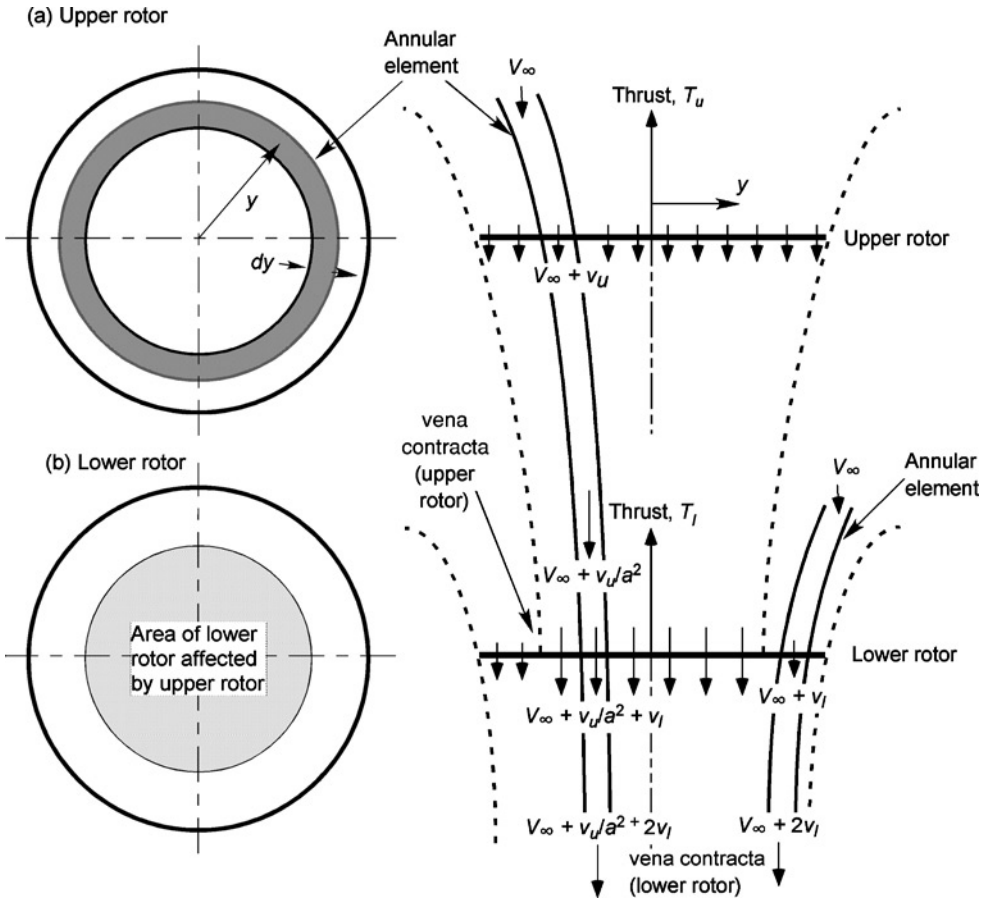

Fig. 1. Flow model used for the BEMT analysis of a coaxial rotor system with the lower rotor operating in the slipstream of the upper rotor.

the wake from the upper rotor is found to contract quickly based on flow visualization (Ref. 24), so using the vena contracta is generally a good assumption for a coaxial rotor system. This issue, however, is discussed in more detail later in this paper.

The BEMT equations are formalized using the assumption that the slipstream wake (outflow) from the upper rotor affects the flow into the lower rotor, but the lower rotor does not produce an induced interference at the upper rotor. This is equivalent to the assumptions made by Lock (Ref. 25) and others (Refs. 4, 26), where the flow velocities of the two rotors are calculated independently and the interference effects are combined by superposition. Such an assumption is reasonable for all but very closely spaced rotors; see Weick (Ref. 14). This assumption, however, does *not* imply that the performance of the upper rotor will be unaffected by the lower rotor. Because the inflow and spanwise loading distributions for both rotors are affected by the overall trim state of the coaxial as a system (i.e., for a given thrust sharing or for a torque balance), then there are always reciprocal effects on the rotors in that the inflow determined on the lower rotor is a function of the loading on the upper rotor and vice versa. In the case where the rotors become very closely spaced, both rotors will share the same inflow and the same resulting levels of performance.

The BEMT can also be generalized in terms of an axial free-stream velocity, say V_∞. This is useful because the final equations also allow an optimum blade design solution to be determined at a prescribed combination of thrust and axial flight speed. Such an analysis would be needed to predict the performance of a proprotor (Ref. 22). The hover case is obtained in the limit as $V_\infty \to 0$.

Consider first the upper rotor of the coaxial system. Momentum theory principles (Refs. 19, 20, 27) can be used to find the incremental thrust on the rotor annulus as the product of the mass flow rate through the annulus and the induced velocity there, i.e., v_u. The mass flow rate over the annulus is

$$d\dot{m} = \rho(V_\infty + v_u)\, dA = 2\pi\rho(V_\infty + v_u) y\, dy \tag{1}$$

where $dA = 2\pi y dy$, so that the incremental thrust on the annulus becomes

$$dT_u = 2\rho\,(V_\infty + v_u)\, v_u\, dA = 4\pi\rho(V_\infty + v_u) v_u y\; dy \tag{2}$$

when assuming the validity of the differential form of the classical momentum theory (i.e., the validity of the Froude–Finsterwalder equation). When converting to standard nondimensional terms, the previous equation can be written as

$$\begin{aligned} dC_{T_u} &= \frac{dT_u}{\rho(\pi R^2)(\Omega R)^2} = \frac{2\rho(V_\infty + v_u) v_u\, dA}{\rho\pi R^2(\Omega R)^2} \\ &= \frac{2\rho(V_\infty + v_u) v_u (2\pi y\; dy)}{\rho\pi R^2(\Omega R)^2} \\ &= 4\lambda\lambda_u r\, dr \end{aligned} \tag{3}$$

where the nondimensional inflow is given by $\lambda = \lambda_u + \lambda_\infty$. Therefore, the incremental thrust coefficient for the rotor annulus can be written as

$$dC_{T_u} = 4\lambda\lambda_u r\; dr = 4\lambda(\lambda - \lambda_\infty) r\; dr \tag{4}$$

The induced power consumed by the annulus is

$$dC_{P_u} = \lambda dC_{T_u} = 4\lambda^2\lambda_u r\ dr = 4\lambda^2(\lambda - \lambda_\infty) r\ dr \tag{5}$$

to a small angle assumption. This latter result assumes no losses from swirl in the wake, which is justified for lightly loaded rotors of any configuration (Ref. 27).

Blade tip loss effects (i.e., the locally high induced losses at the blade from the formation of the tip vortex) can be accounted for in the BEMT by using the Prandtl tip-loss function (Ref. 20). This loss is expressed in terms of a correction factor, F, as

$$F = \left(\frac{2}{\pi}\right)\cos^{-1}\left(\exp(-f)\right) \tag{6}$$

where f is given in terms of the number of blades, N_b, and by the radial position of the blade element, r, by

$$f = \frac{N_b}{2}\left(\frac{1-r}{r\phi}\right) \tag{7}$$

and where ϕ is the inflow angle (equal to $\lambda(r)/r$ with a small angle assumption). In application, the Prandtl function modifies the Froude–Finsterwalder equation to

$$dC_T = 4F\lambda\lambda_u r\ dr \tag{8}$$

Now, using the conventional blade-element theory (i.e., the circulation theory of lift) with small angle assumptions, then the incremental thrust produced on the same annulus of the disk is

$$dC_{T_u} = \tfrac{1}{2}\sigma_u\, C_l r^2\, dr = \tfrac{1}{2}\sigma_u\, C_{l_\alpha}(\theta_u - \phi) r^2\, dr = \frac{\sigma_u\, C_{l_\alpha}}{2}\left(\theta_u r^2 - \lambda r\right) dr \tag{9}$$

where θ_u is the blade pitch distribution on the upper rotor, which may include the zero-lift angle(s) of the blade sections. Therefore, equating the incremental thrust coefficients from the momentum and blade-element theories (i.e., using Eqs. (4) and (9)) gives

$$\frac{\sigma_u\, C_{l_\alpha}}{2}\left(\theta_u r^2 - \lambda r\right) = 4F\lambda(\lambda - \lambda_\infty) r \tag{10}$$

or rearranging in terms of λ gives the quadratic

$$\lambda^2 + \left(\frac{\sigma_u\, C_{l_\alpha}}{8F} - \lambda_\infty\right)\lambda - \frac{\sigma_u\, C_{l_\alpha}}{8F}\theta_u r = 0 \tag{11}$$

This equation in the unknown λ has the solution

$$\lambda(r, \lambda_\infty) = \sqrt{\left(\frac{\sigma_u\, C_{l_\alpha}}{16F} - \frac{\lambda_\infty}{2}\right)^2 + \frac{\sigma_u\, C_{l_\alpha}}{8F}\theta_u r} - \left(\frac{\sigma_u\, C_{l_\alpha}}{16F} - \frac{\lambda_\infty}{2}\right) \tag{12}$$

where $\lambda_u = \lambda - \lambda_\infty$.

Equation (12) can be solved numerically at a series of discretized elements that are distributed radially over the rotor disk (Ref. 20). Because F is a function of the inflow λ, this latter equation is solved using fixed-point iteration by first calculating λ using $F = 1$ (corresponding to $N_b \to \infty$) and then finding F from Eq. (6) and recalculating λ from Eq. (12). Convergence is rapid, typically taking only 5–10 iterations per element.

The same mathematical principles can be applied to the analysis of the lower rotor of the coaxial. However, in this case it is assumed that the inner part of the lower rotor operates in the vena contracta of the upper rotor (see Fig. 1) with a fully developed slipstream velocity there and a maximum change in its momentum. The slipstream velocity in the streamtube of the upper rotor can be defined on the basis of an assumed radial contraction of the wake, a, i.e., the contracted wake area is $A_c = \pi a^2 R^2$. In the ideal case, $a = 2^{-1/2} = 0.707$ or $A_c/A = 0.5$. In this particular case, the inner area of the lower rotor encounters incoming contracted differential streamtubes with velocity $V_\infty + 2v_u$, or with velocity $V_\infty + (A/A_c)v_u$ or $V_\infty + v_u/a^2$ in the more general case where the wake contraction from the upper rotor is otherwise specified empirically by using A_c or a.

Following the same steps as done for the upper rotor, for points on the lower rotor disk that are affected by the slipstream from the upper rotor (i.e., for $r \le a$), the inflow distribution on the lower rotor is given by solving

$$\lambda(r, \lambda_\infty) = \sqrt{\left(\frac{\sigma_l\, C_{l_\alpha}}{16F} - \frac{\lambda_\infty + \lambda_u/a^2}{2}\right)^2 + \frac{\sigma_l\, C_{l_\alpha}}{8F}\theta_l r} - \left(\frac{\sigma_l C_{l_\alpha}}{16F} - \frac{\lambda_\infty + \lambda_u/a^2}{2}\right) \quad \text{for } r \le a \tag{13}$$

where θ_l is the blade pitch distribution over the lower rotor. In this case $\lambda_l = \lambda - \lambda_\infty$. Note that the contracting streamtubes must be mapped from originating points on the upper rotor to receiving points on the lower rotor within the inner area that is affected by the wake, i.e., a streamtube emanating from radial point r on the upper rotor will map to new radial point ar on the lower rotor.

For points outside this area that are unaffected by the slipstream from the upper rotor (i.e., for $r > a$), the inflow distribution is given by solving

$$\lambda(r, \lambda_\infty) = \sqrt{\left(\frac{\sigma_l\, C_{l_\alpha}}{16F} - \frac{\lambda_\infty}{2}\right)^2 + \frac{\sigma_l\, C_{l_\alpha}}{8F}\theta_l r} - \left(\frac{\sigma_l\, C_{l_\alpha}}{16F} - \frac{\lambda_\infty}{2}\right) \quad \text{for } r > a \tag{14}$$

The three equations (Eqs. (12)–(14)), therefore, give an approximation to the inflow distribution at discrete radial positions over both the upper and lower rotors for any specified blade pitch, blade twist distribution, planform shape (i.e., chord or solidity distribution), and airfoil section (i.e., implicitly through the effect of lift-curve-slope and zero-lift angle of attack).

When the spanwise inflow distributions are obtained, the rotor thrust and power (induced plus profile) for each rotor may then be found by numerical integration across each respective rotor disk. For the upper rotor, the thrust coefficient is

$$C_{T_u} = \int_{r=0}^{r=1} dC_{T_u} = \frac{1}{2}\int_r^1 \sigma_u C_l r^2\, dr \tag{15}$$

and the power coefficient (sum of induced and profile sources) is

$$C_{P_u} = \int_{r=0}^{r=1} \lambda_u\, dC_{T_u} + \int_0^1 \frac{1}{2}\sigma_u\, C_d r^3\, dr \tag{16}$$

where C_d is the sectional profile drag coefficient. In the first instance, C_d can be assumed equal to C_{d_0} without much loss of accuracy up to moderate values of blade loading coefficient. Normally, however, the full range of lift and drag coefficients for specific airfoil sections would be incorporated into the analysis using a table lookup approach. For the lower rotor, the thrust and power coefficients are

$$C_{T_l} = \int_{r=0}^{r=1} dC_{T_l} = \frac{1}{2}\int_0^1 \sigma_l C_l r^2\, dr \tag{17}$$

and

$$C_{P_l} = \int_{r=0}^{r=1} \lambda_l \, dC_{T_l} + \frac{1}{2} \int_0^1 \sigma_l \, C_d \, r^3 dr \tag{18}$$

respectively, where it should be noted that $\sigma_u \neq \sigma_l$, in general.

The two rotors can then be trimmed (numerically) by adjusting their respective reference (i.e., collective) pitch angles to meet the specified total system thrust (i.e., using $C_T = C_W = C_{T_u} + C_{T_l}$) or to any other specified rotor thrust sharing condition. More often, the rotors will be operated at a torque (or power) balanced condition (i.e., $C_{P_u} - C_{P_l} = 0$) where the blade pitch or thrust sharing is not assumed a priori, and such values become an output of the trim process. Note that the solutions for the inflow on the upper and lower rotor are intrinsically coupled by the assumed trim state.

Validation of the Coaxial Rotor Model

For single rotors, the BEMT approach is already known to have good validity for rotor airloads predictions when compared to more sophisticated aerodynamic models, except perhaps at the extreme blade tip and inner root regions (Ref. 20). In the case of a coaxial rotor, the BEMT can be expected to become increasingly invalid in the region where the blade tip vortices that convect along the wake boundary from the upper rotor impinge on the lower rotor. While a good approximation to the tip-loss effect on the radial inflow distribution (on both the upper and lower rotors) can be made using Prandtl's circulation-loss function, there is no equivalent "loss" function to represent the local induced losses where the wake boundary from the upper rotor interacts with the lower rotor. Therefore, the BEMT would generally be expected to underpredict the aggregate of the induced and viscous losses. Rectifying this limitation requires a better treatment of the wake–rotor interaction problem, at a minimum by using vortex theory (Refs. 12, 28), and probably by using CFD in the form of Reynolds-averaged Navier–Stokes (RANS) methods (Ref. 13) to capture the viscous losses. However, such vortex wake–blade interaction problems on coaxials, and the quantification of their effects on blade loads and overall rotor efficiency, remain largely unstudied.

Hovering flight

The BEMT was validated against the measurements made by Harrington (Ref. 29), which were made using two sets of nominally full-scale rotors operating in the hovering condition. Both rotors were 25 ft (7.62 m) in diameter with untwisted blades. Rotor 1 had two blades per rotor that were tapered in planform (approximately a 3:1 taper ratio) and corresponding thickness, with a thrust-weighted solidity σ, of 0.027 (i.e., $2\sigma = 0.054$ when operated as a coaxial). Rotor 2 had two blades per rotor that were tapered only in thickness-to-chord ratio with a solidity of 0.076 (i.e., $2\sigma = 0.152$ as a coaxial). Rotor 1 had an interrotor plane spacing of 0.186 R, and rotor 2 had a rotor spacing of 0.16 R.

The simple momentum theory (Refs. 20, 22, 23, 27, 30) was used as a baseline for comparison with the BEMT results. The theoretical power coefficient for the single rotor system can be calculated using the empirically modified SMT, i.e.,

$$C_P = \frac{\kappa C_T^{3/2}}{\sqrt{2}} + \left(\frac{\sigma \, C_{d_0}}{8} \right) \tag{19}$$

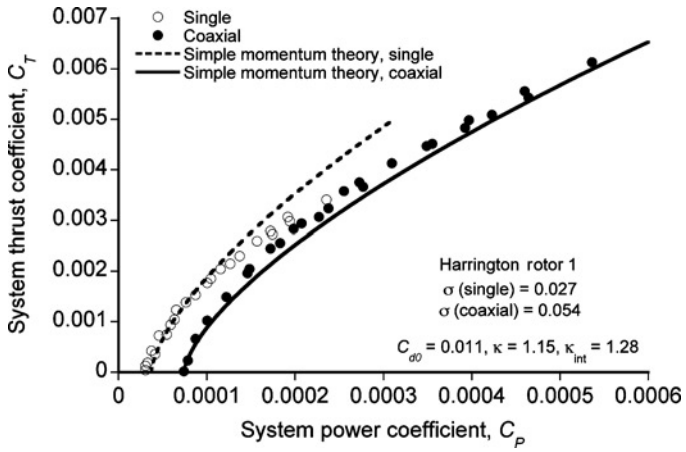

Fig. 2. Predictions using SMT for single and coaxial rotors against measurements of thrust and power. Measurements for Harrington rotor 1.

The corresponding power coefficient for the coaxial rotor system can be calculated using

$$C_P = \frac{\kappa_{\text{int}} \kappa (C_{T_u} + C_{T_l})^{3/2}}{2} + \left(\frac{\sigma C_{d_0}}{4} \right) = \frac{\kappa_{\text{int}} \kappa C_W^{3/2}}{2} + \left(\frac{\sigma C_{d_0}}{4} \right) \tag{20}$$

where κ_{int} represents the rotor-on-rotor induced power interference (Ref. 23) and only the leading term of the profile drag is assumed.

Results for the Harrington rotors 1 and 2 are shown in Figs. 2 and 3, respectively, where it can be seen that the agreement of SMT with the measurements is fairly reasonable, but this theory does not accurately predict the rotor performance over its full range of operating conditions. Note that it also always requires the a priori specification of κ, κ_{int}, and C_{d_0}, which must be assumed or derived empirically by baselining predictions against some known rotor performance. In this regard, the modified SMT really only has a postdictive modeling capability.

Results using the BEMT as formulated for the Harrington rotors 1 and 2 are shown in Figs. 4 and 5, respectively. With the BEMT, only values for the profile drag coefficient need to be specified. In this case, it was assumed that $C_d = C_{d_0} =$ constant to show the effects of improving the

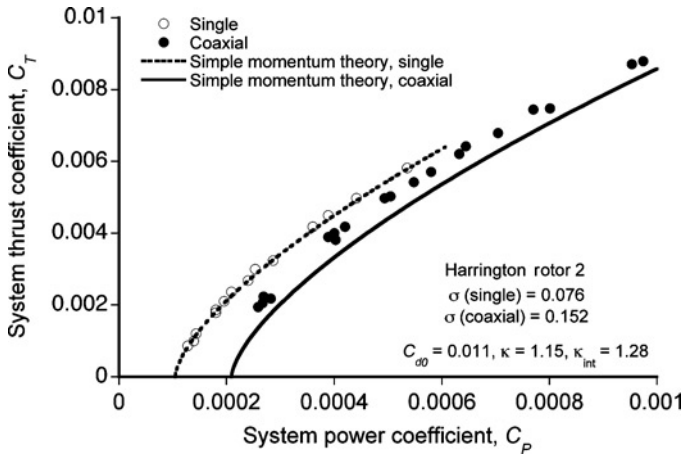

Fig. 3. Predictions using SMT for single and coaxial rotors against measurements of thrust and power. Measurements for Harrington rotor 2.

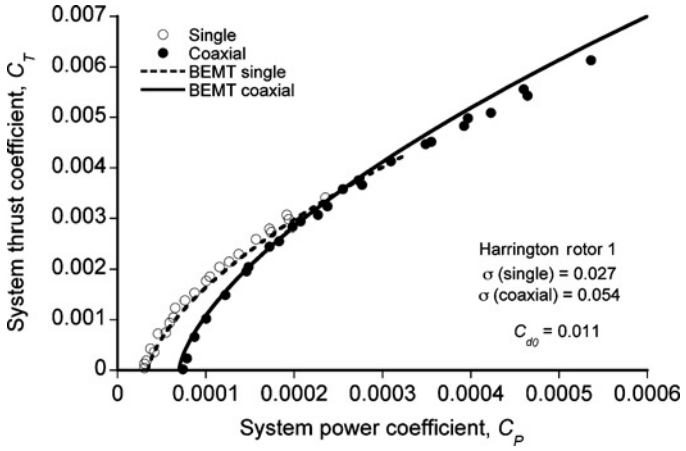

Fig. 4. Validation of the BEMT for single and coaxial hovering rotors against measurements of thrust and power. Measurements for Harrington rotor 1 (results obtained at a torque balance).

modeling of just the induced losses. Further quantitative improvements at higher thrust coefficients can be obtained by assuming $C_d = C_d(\alpha)$ based on two-dimensional measurements for the NACA 0012 airfoil. In either case, BEMT predictions were found to be in good agreement with measured rotor performance and were clearly superior to those obtained using the SMT (cf. Figs. 2 and 3). This is mainly because with the BEMT the nonuniform radial distribution of induced losses over the disk is being resolved, along with a better approximation to the blade tip losses, and so the BEMT gives a much better overall prediction of the performance of the coaxial rotor as a function of its operating state and load sharing.

BEMT predictions of the induced power factor for one of the rotors operating in isolation compared to the Harrington rotor 1 coaxial are shown in Fig. 6 versus blade loading coefficient C_T/σ. With blade tip losses, the induced power factor, κ, of the single rotor is about 1.10, although the BEMT shows that this value varies slightly with C_T/σ. (The predictions of power are sensitive to κ.) The BEMT predicts that induced power factor resulting from rotor-on-rotor interference alone (i.e., κ_{int}) is about 1.28 at the higher thrust levels, and this value is consistent with the result from the SMT solutions (Refs. 22, 23).

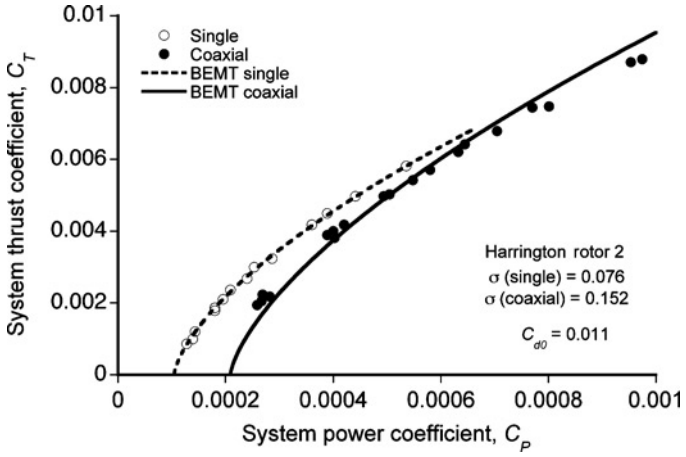

Fig. 5. Validation of the BEMT for single and coaxial hovering rotors against measurements of thrust and power. Measurements for Harrington rotor 2 (results obtained at a torque balance).

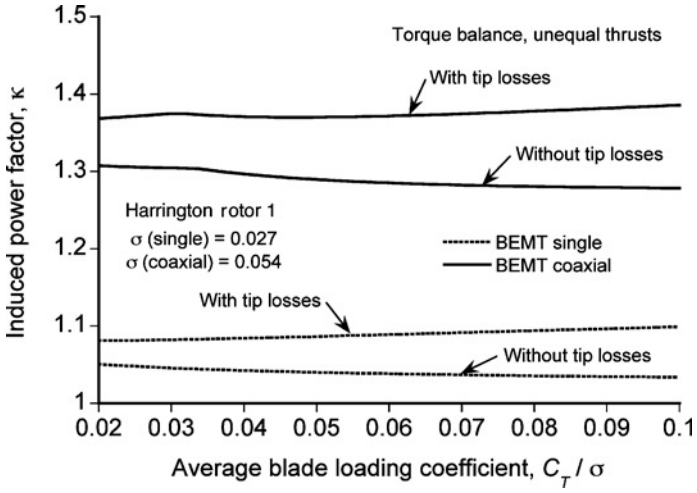

Fig. 6. Variation in the induced power factor for single and coaxial rotors, with and without tip losses (results obtained at a torque balance).

As previously mentioned, a primary issue with a coaxial rotor is that the wake from the upper rotor is ingested into the lower rotor, hence affecting significantly the distribution of airloads there. The physics of the wake is illustrated in Fig. 7, which show results from a free-vortex method (FVM) (Refs. 28, 31, 32). Note that the wake from the upper rotor contracts smoothly into the lower rotor, and its helicoidal structure is mostly preserved as it is convected through and below the lower rotor. This calculation is consistent with flow visualization experiments, such as those of McAlister et al. (Ref. 6) and Taylor (Ref. 24), where the upper and lower rotor wakes appear to remain relatively distinct as they merge. However, the two sets of wakes still interact with each other, and the resulting flow downstream is not necessarily one that can be obtained by linear superposition. The predicted radial contraction of the wake from the upper rotor in this case is about 80% (compared to the ideal wake contraction of 70.7%) and is similar to the values found on

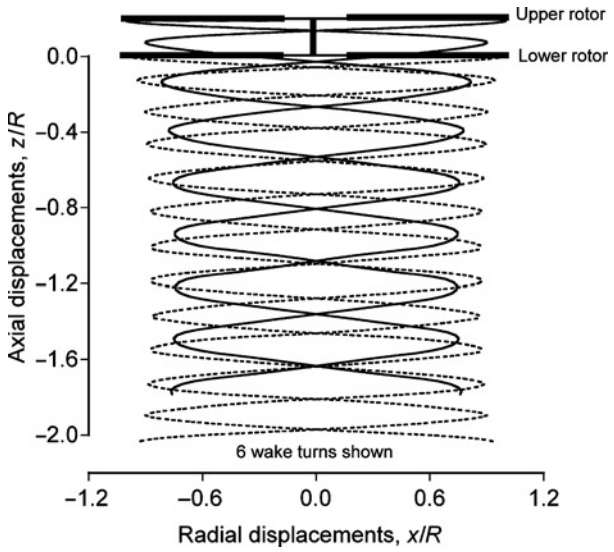

Fig. 7. Predicted vortex wake geometry for a coaxial rotor showing how the tip vortices from the upper rotor are ingested into the lower rotor.

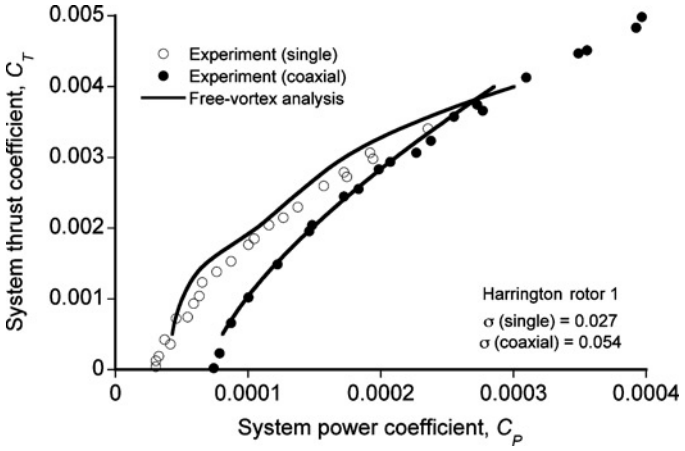

Fig. 8. Validation of the FVM against measurements of thrust and power for the Harrington rotor 1 (results obtained at a torque balance).

isolated hovering rotors (which are typically between about 78% and 82% depending on the rotor type and operating state).

Results from the FVM were also compared with the measured thrust and power for Harrington's rotors 1 and 2, as shown in Figs. 8 and 9. Note that the FVM predictions are in generally good agreement with the measurements and are also in good agreement with the BEMT (Fig. 4). The FVM results used aerodynamic coefficients for the NACA 0012 airfoil.

There are almost no measured spanwise airloads on coaxial rotors, and none in Harrington's tests. There are some estimates of the spanwise loadings on contrarotating dual propellers, as derived from wake measurements (Ref. 33), but no blade loads have been measured directly. Therefore, spanwise airloads predicted by the FVM were used to compare directly with the BEMT. The FVM calculations were performed "in the blind," the analyst having only the rotor geometry and its operating state, but no results from the BEMT or the experiment were given about the predicted performance, load sharing, or expected spanwise loading distributions. For this study, the Harrington rotor 1 was used with a net system C_T of 0.004 at a torque balance.

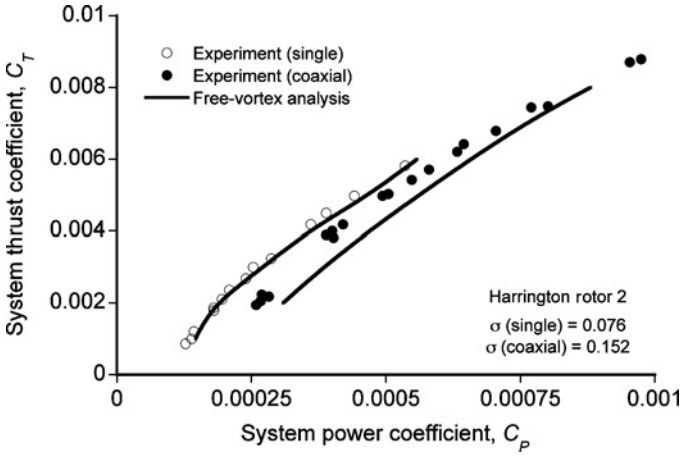

Fig. 9. Validation of the FVM against measurements of thrust and power for the Harrington rotor 2 (results obtained at a torque balance).

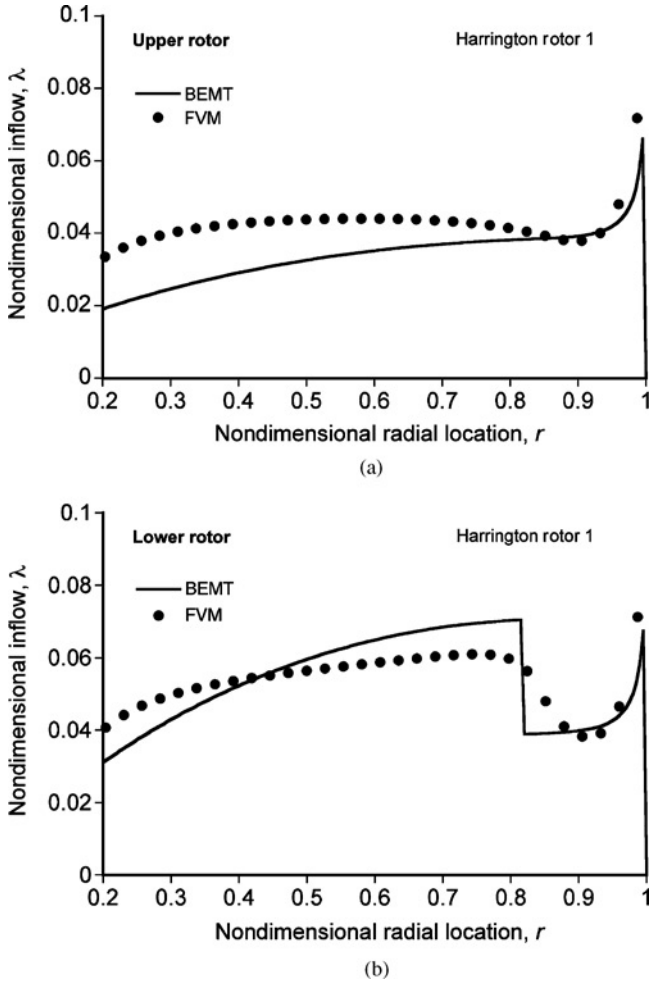

Fig. 10. Predicted spanwise distribution of inflow for the upper and lower rotors using the BEMT and the FVM. Results for Harrington rotor 1, $C_T = 0.004$ (results obtained at a torque balance).

Results for the inflow distribution predicted by the BEMT and FVM are shown in Fig. 10 for the upper and lower rotors, respectively. In this case, for the BEMT predictions the wake from the upper rotor was assumed to contract to $a = 0.82$, consistent with the predictions made by the FVM. No blade root cutout losses were included in the BEMT analysis. Note that the inflow at the lower rotor is substantially affected by the outflow from the upper rotor, with a higher inflow over the inboard regions of the lower rotor. The lower rotor less influences the inflow at the upper rotor, but there was still some effect on power compared to what the upper rotor would produce in isolation at the same thrust, i.e., when decoupled from the lower rotor.

Overall, the agreement between the predictions from the BEMT and FVM is clearly quite reasonable in both magnitude and in form, although perhaps less so in detail; this is partly because the results are obtained for a torque balance not a thrust balance (see next). More importantly however, recall that the BEMT is essentially a two-dimensional theory compared to the FVM, which gives three-dimensional flow field predictions (i.e., all three components of the flow field are computed, and blade section-on-section aerodynamic interference effects are also modeled). Note that the Prandtl tip loss function gives a good definition of the high inflow at the blade tips.

The radial thrust distributions on the coaxial rotor are shown in Fig. 11 for the upper and lower rotors, respectively. The agreement

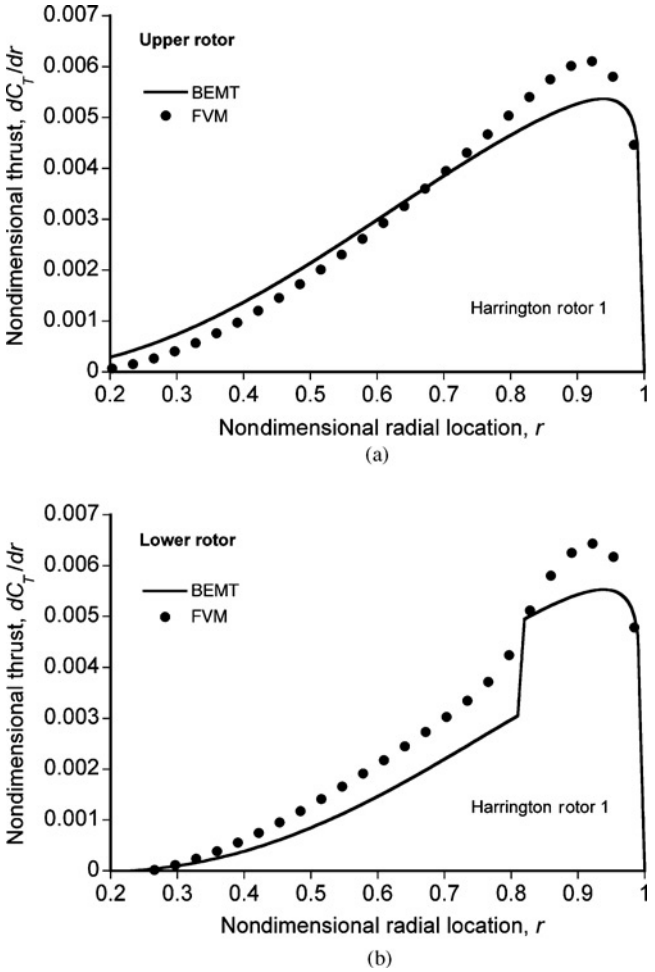

Fig. 11. Predicted spanwise distribution of thrust for the upper and lower rotors using the BEMT and the FVM. Results for Harrington rotor 1, $C_T = 0.004$ (results obtained at a torque balance).

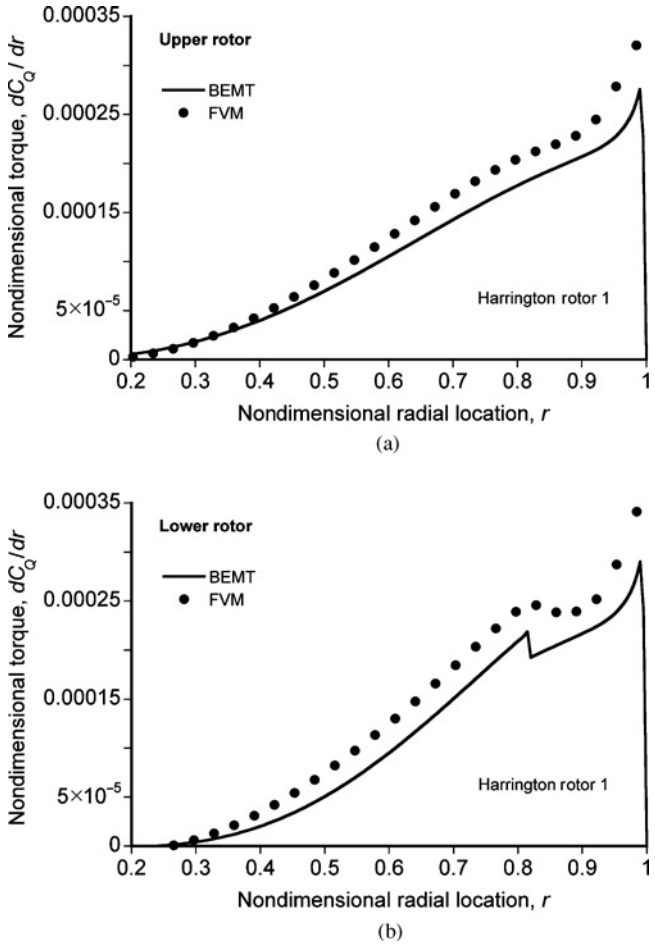

Fig. 12. Predicted spanwise distribution of torque for the upper and lower rotors using the BEMT and the FVM. Results for Harrington rotor 1, $C_T = 0.004$ (results obtained at a torque balance).

here between the BEMT and the FVM is seen to be quite good. The corresponding torque distributions on the coaxial are shown in Fig. 12, which are again quite good. Note that the collective pitch on both rotors was adjusted to give a torque balance, so the net areas under the torque curves are equal in both cases. Again, it can be seen that the effect of the wake slipstream from the upper rotor is to alter the spanwise loading, especially over the region near the slipstream boundary, which in this case is at about 82% span.

Furthermore, note that for a torque balance, the upper rotor carries a greater fraction of the total system thrust ($C_{T_u}/C_{T_l} \approx 1.25$ in this case). This is because the induced losses would otherwise be higher on the lower rotor, so the upper rotor must operate at a higher thrust to counter the net torque on the coaxial as a system. The effects of the slipstream from the upper rotor can also be seen in the thrust distribution in Fig. 11(b), which is substantially reduced inboard compared to that on the upper rotor, and becomes slightly negative well inboard. Outside of the region affected by the slipstream, the blade thrust distribution quickly recovers to values that are consistent with those found on the upper rotor.

Overall, these results show that the BEMT and FVM predictions agree quite well, especially bearing in mind that the BEMT is computationally just a few seconds of time versus several minutes for a FVM solution. These results also help to validate the various assumptions made in the development of the BEMT.

Axial flight

For axial flight conditions, the BEMT was validated against measurements made for propellers. The performance characteristics of both single and coaxial propellers were examined, and measurements were sought at the rotational tip speeds, tip Mach numbers, and forward speed ratios that would be typical of those encountered by a proprotor.

Single propeller. Representative validation results against a NACA high-speed propeller test (Ref. 34) are shown in Figs. 13 and 14 for the thrust and power, respectively. The thrust and power coefficients have been converted from propeller nomenclature into conventional helicopter rotor nomenclature. Note that propeller performance is conventionally plotted versus "advance ratio" J; the values of "forward speed ratio" and J are then related simply by the formula: forward speed ratio $= J/\pi$. This NACA propeller has thin blades (about 8% thickness-to-chord ratio) compared to a proprotor, but the data provide a good test case for assessing both the capabilities and limitations of the BEMT because the propeller was operated at the higher forward speeds (and forward speed ratios) that took the blade tips into the transonic flow range.

Figure 13 shows the variation of thrust (in terms of blade-loading coefficient) versus forward speed ratio as a set of curves for increasing values of fixed blade pitch. From zero forward speed and low blade pitch, the thrust decreases almost linearly with increasing V_∞. Eventually, the

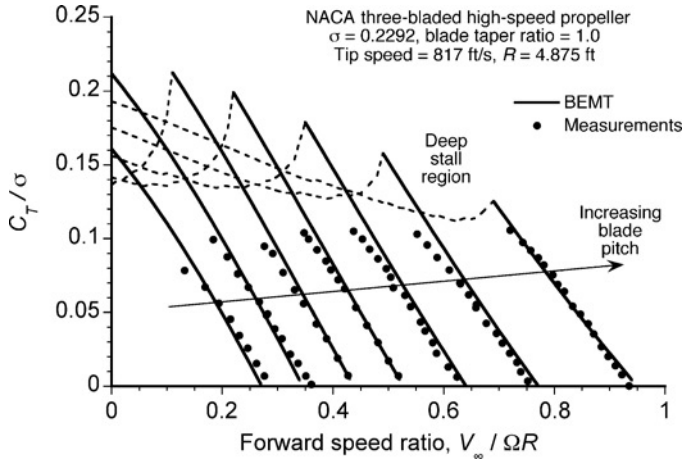

Fig. 13. Validation of the BEMT with thrust measurements on a NACA high-speed propeller as a function of forward speed ratio. (- - - - represents predictions with blade stall.)

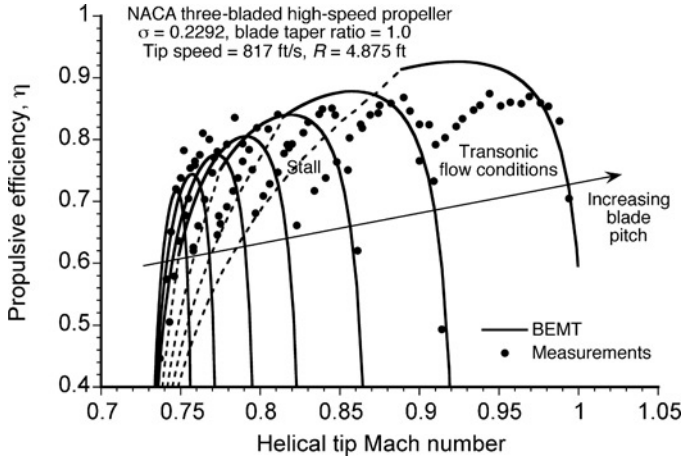

Fig. 15. Predictions and measurements of propulsive efficiency of a NACA high-speed propeller as a function of helical Mach number. (- - - - represents predictions with blade stall.)

propeller produces negative thrust (i.e., the brake state is reached) unless the blade pitch is increased to higher values. At low forward speeds with higher pitch, the blades are initially stalled, so the propeller generates some thrust but needs high power (Fig. 14). In fact, the measurements showed that in this regime the thin blades of this propeller experienced stall flutter, and could not operate here continuously. Increasing V_∞ for a fixed blade pitch and tip speed causes the flow on the blades to attach, and thereafter the propeller produces thrust and the power requirements significantly decrease, the propulsive efficiency also increasing. Again, the thrust on the propeller is seen to decrease quickly with V_∞ when the blade pitch is held constant. The BEMT was shown to give very good agreement with thrust measurements at each blade pitch.

Figure 14 shows that the power curves become increasingly steeper with increasing values of V_∞. This is because induced power losses become a smaller fraction of the total system losses, so the overall performance of the propeller is increasingly determined by the profile drag losses on the blades rather than by the operating thrust. The underprediction of power at higher values of V_∞ arises partly because of the difficulties in representing the three-dimensional nonlinear aerodynamics of the blade tip sections at higher angles of attack, especially in transonic flow. These transonic effects include increases in drag coefficient, a reduction in lift-curve slope, and a change in the zero-lift angle of attack, effects that are compounded by tip-relief effects. Despite these modeling challenges, the BEMT predictions were found to be in good agreement with the measurements over a fairly wide range of operating conditions.

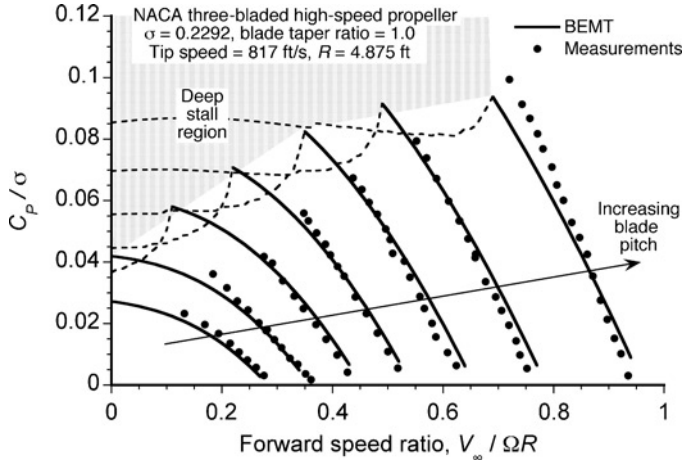

Fig. 14. Validation of the BEMT with power measurements on a NACA high-speed propeller as a function of forward speed ratio. (- - - - represents predictions with blade stall.)

Note that while the performance of the propeller is bounded on one side by losses in thrust (and hence efficiency) resulting from blade stall at a given blade pitch, at higher forward speed the performance is limited by growing compressibility effects as the blade tip sections eventually experience drag divergence and also lose lift. Hence, the maximum values of C_T/σ that can be produced decreases as the areas on the blades affected by compressibility grow with increasing V_∞; C_P/σ also increases rapidly here from the increases in section drag. The effects of tip relief, however, modify the relationships between these parameters and the angles of attack, so the net result (in this case at least) is that the BEMT tends to underpredict the power. In fact, the relatively high speeds encountered by the blade elements in this propeller test (which propagate well into the transonic regime) provide a good challenge for any kind of rotor modeling, not just with the BEMT. This is because the airfoil section characteristics (lift and drag) are highly nonlinear, and become sensitive to small inaccuracies in the predictions of the induced velocities and local angles of attack.

Of course, a sensitive indicator to all of these aerodynamic issues is the propulsive efficiency of the propeller, which is best exposed when the efficiency curves are plotted versus the helical Mach number at the tip of the blade, as shown in Fig. 15. Note that the helical Mach number is determined by the resultant of the rotational and translational (i.e., axial) velocities. While the overall envelope defining the peak propulsive efficiency seems to be reasonably well predicted by the BEMT (at least for this particular propeller), the shapes of the various efficiency curves near their peak are obviously predicted less satisfactorily. As previously alluded to, this is because of the challenges in using blade-element models to predict the three-dimensional nonlinear aerodynamic characteristics of the blade tip sections in transonic flow and beyond. Despite these challenges, the BEMT results were found to be in substantially good overall agreement with the performance measurements made for this propeller.

Coaxial propeller. The contrarotating coaxial propeller case obviously poses a more significant challenge for the BEMT because now the simultaneous performance of both propellers must be predicted accurately. In

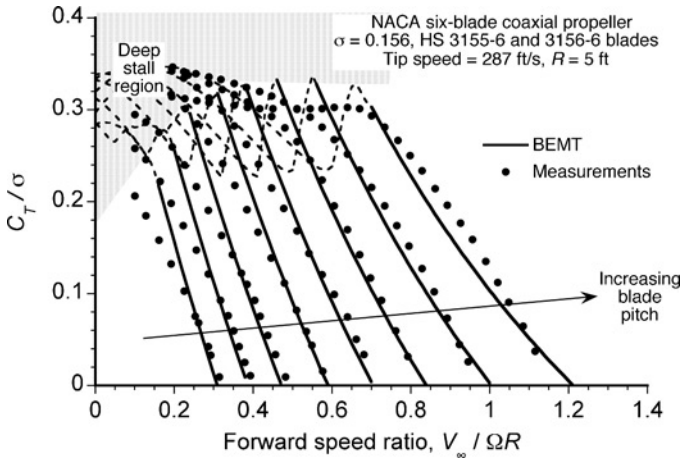

Fig. 16. Validation of the BEMT with thrust measurements for a NACA coaxial propeller as a function of forward speed ratio. (- - - - represents predictions with blade stall.)

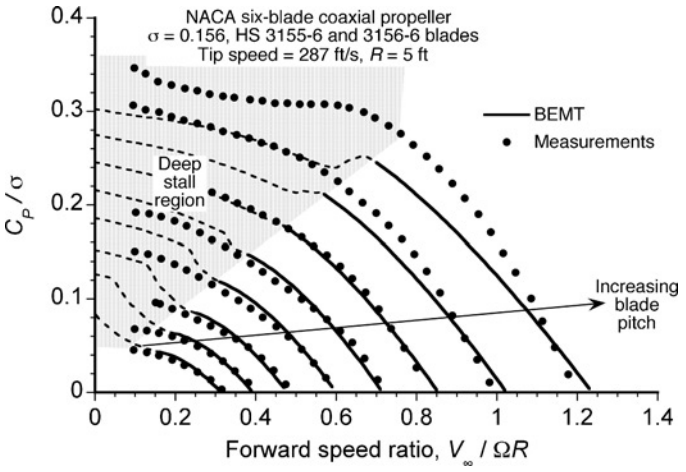

Fig. 17. Validation of the BEMT with power measurements for a NACA coaxial propeller as a function of forward speed ratio. (- - - - represents predictions with blade stall.)

particular, the induced slipstream effects of the front propeller on the rear propeller must be precisely predicted, and of course this problem poses a good challenge for any type of aerodynamic model. Unfortunately, there are very few measurements of coaxial propeller performance at the full-scale flight conditions that would be typical of a proprotor. The comprehensive results obtained by Biermann and Hartman (Ref. 35) are for nominally full-scale coaxial propellers, but they were operated at subscale rotational tip speeds and tip Mach numbers. Nevertheless, the tests were conducted at the high forward speed ratios that still took the helical Mach numbers on the propeller tips just into the transonic flow region, thereby providing some good data for validation. Pairs of two- and three-bladed coaxial propellers were tested. The pitches of the blades were fixed and were set with an appropriate differential pitch to give an approximate torque balance near maximum propulsive efficiency.

Figure 16 shows the variation of total thrust on a three-bladed contrarotating coaxial pair (i.e., a total of six blades) versus forward speed ratio as a set of curves for increasing values of blade pitch, as in the manner shown previously in Fig. 13 for the single propeller. The blade section characteristics were specified using a method similar to that described in Ref. 36 for the Clark Y airfoils used on this propeller, but with the addition of poststall modeling. The overall agreement between the BEMT results and the measurements is seen to be relatively good, although there are perhaps more deficiencies compared to the results found with the single propeller. These predictive deficiencies are particularly apparent at higher values of C_T/σ and at higher forward speed ratios, where the effects of stall and compressibility both start to become apparent. In this case, both of these physical effects must be predicted equally well on both the front *and* rear propellers to achieve overall predictive success, and this depends on the relative load sharing between the two propellers at each operating point.

Figure 17 shows the corresponding predictions of power as a function of forward speed ratio for a range of blade pitch angles. The power curves are clearly more sensitive to variations in V_∞ than was found for the single propeller (cf. Fig. 14). Predictions of power are seen to be good at the lower and intermediate forward speed ratios, but become less satisfactory at the higher thrusts and higher forward speed ratios, partly for the reasons explained previously—this outcome was also noted in Ref. 36. In addition, the drag from the inner parts of the blade cross sections (which are circular) is significant. These problems are compounded by the difficulties in predicting accurately the angles of attack at all of the blade elements that result from rotor-on-rotor interference effects, which are also a function of the assumed wake contraction. Varying the wake contraction parameter a was found to improve some of the predictions, although this change did not universally rectify the discrepancies over the entire working range of the propeller. Another issue is that for these conditions the small angle assumptions made in the development of the equations in the BEMT become increasingly questionable, and for very high forward speed ratios (above 1.5) the assumptions will become invalidated. If predictions in this regime were deemed important, then the BEMT must be reformulated to remove all of the small angle assumptions.

Rotor Plane Separation Effects

The BEMT (as developed) provides no formal mathematical mechanism for assessing the aerodynamic effects of rotor plane separation distance. It has been previously stated that one assumption in the development of the BEMT is that the lower rotor operates in the fully developed slipstream of the upper rotor. In practice, this means that the wake from the upper rotor has essentially undergone its maximum contraction (and so has reached its asymptotic wake velocity) before being ingested into the lower rotor. In the BEMT, this contraction ratio can be specified theoretically or empirically, as previously discussed.

To further examine this issue, the FVM was exercised for several rotor plane separations. The Harrington rotor 1 was used as a baseline, although other rotor systems were also examined. The relationship between wake contraction and the rotor plane separation distance as predicted by the FVM is shown in Fig. 18. The results confirm that in the limit, as the rotors become more significantly separated, the wake contraction does indeed approach an asymptotic value. Practical helicopter rotor spacings will generally be within the range where the asymptotic wake contraction has been reached, although coaxial propellers and proprotors will typically have lower rotor spacings. The validity of the BEMT, therefore, must generally be established through confidence in validation.

The corresponding results for the induced power factors are shown in Fig. 19 for the range of computed wake contractions. Note that the induced power factor also increases with decreasing rotor plane separation, as would be expected based on SMT considerations (Ref. 23). The BEMT was found to underpredict the induced power factors at the lower rotor spacings compared to those from the FVM. This can be expected because the nonuniformity of the inflow and tip losses is more accurately

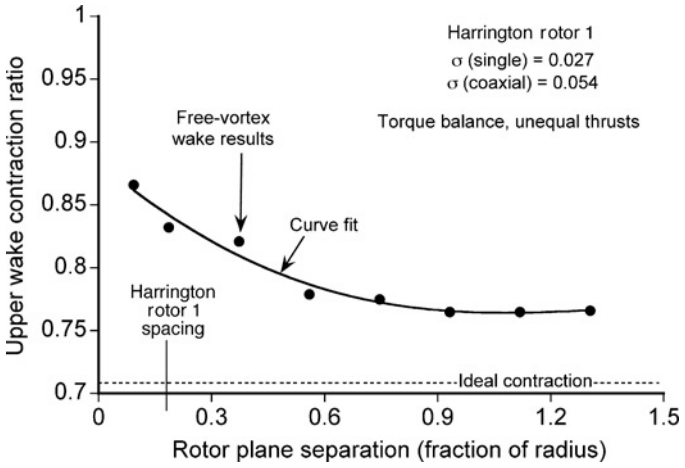

Fig. 18. Predicted relationship between the wake contraction from the upper rotor into the lower rotor as a function of rotor plane separation distance. (Harrington rotor 1.)

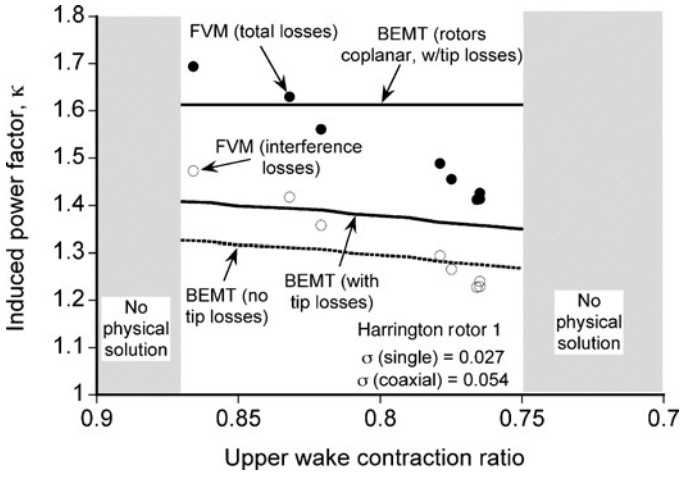

Fig. 19. Predicted relationship between the induced power factor and the wake contraction from the upper rotor. (Harrington rotor 1.)

accounted for in the FVM, and eventually for very close spacings the inflow into the lower rotor begins to affect the flow and resulting performance of the upper rotor. This confirms that part of the underprediction of power on the coaxial propeller (Fig. 17) is probably tied also to the inadequacy of modeling this effect.

Note that in the limit of zero rotor spacing, the upper and lower rotors will share the same values of induced velocity, and the induced losses of the system will then reach their maximum. In this case, the BEMT must be modified such that the spanwise distributions of λ_u and λ_l become identical (also with a wake contraction ratio of unity), and the predictions in this case were found to be in better agreement with the FVM results.

Optimum Hovering Coaxial Rotor

An outcome of formulating a BEMT analysis for a coaxial rotor system is that it allows the blade twist and planform shapes on the upper and lower rotors to be designed theoretically to give a specified level of performance, including a definition of the conditions needed to operate the coaxial rotor at maximum efficiency (i.e., to achieve minimum induced, profile, and rotor-on-rotor interference losses). This approach, therefore, can be used to seek an optimum coaxial rotor design for a given operating state. For a single rotor in hovering flight, Gessow (Ref. 18) and Gessow and Myers (Ref. 19) showed that its "optimum" design must use hyperbolically twisted blades to obtain uniform inflow and minimum induced losses. This twist must then be combined with hyperbolically tapered blade chords to produce a condition where all the airfoil sections on the blades also operate at their best lift-to-drag ratios (or close to this condition) to realize minimum profile losses. The resulting optimum blade design, however, is not realizable in practice (although it can be closely approximated by using linear blade twist and taper distributions), nor is this blade shape optimum for forward flight (i.e., as an edgewise flying rotor). Nevertheless, the classic optimum rotor principles provide design goals to help extract the best rotor performance for a given flight condition.

The objective here was to seek the equivalent optimum blade design for the coaxial rotor system. From the BEMT equations previously derived, the solution for the inflow distribution over the upper and lower rotors is given by Eqs. (12)–(14). Other physical factors that can affect coaxial rotor performance include a thrust (or power) recovery effect through the removal of some swirl losses in the downstream wake, although this effect is important only at very high values of disk loading and at the high rotational speeds such as those used on propellers, but even then the losses are relatively small. Therefore, wake swirl can be justly neglected as a second-order effect when finding an initial approximation to an optimum coaxial rotor design, although the effects would be intrinsically included in any optimization process using, for example, a FVM.

On the upper rotor, it is obvious that the inflow distribution must be uniform to realize the minimum induced losses. This is equivalent to producing a uniform disk loading and a linear thrust per unit span starting from zero at the rotational axis to a maximum value at the blade tip (assuming no tip losses). Therefore, Eq. (12) can easily be solved for the distribution of $\theta_u(r)$ that will achieve this goal. By inspection, it is apparent that the blade twist distribution must be hyperbolic, i.e., of the form $\theta_u = \theta_{u_{\text{tip}}}/r$, if uniform disk loading is to be achieved.

On the lower rotor, the inflow distribution cannot be made uniform, at least not without leading to aerodynamic inefficiency, and it will become clear that this should not be the goal anyway. In fact, the distribution of inflow to achieve minimum induced losses is the condition where the inflow *inside* the region affected by the upper rotor is made uniform *and* the inflow is also made uniform *outside* this region, i.e., *both* regions over the disk now have uniform inflow but *not* of the same values. This result is consistent with the SMT solution (Refs. 22, 23). The optimum loading condition in this case (i.e., minimum induced power), however, is still a uniform disk loading and a linear thrust distribution over the blade span.

The procedure used to find the shape of the blades for the optimum coaxial rotor can be undertaken numerically using the BEMT. Remember that the final result obtained for any given coaxial rotor is really only a point design (i.e., the blade pitch distribution, planform, and so on depend on the specific operating state of the coaxial rotor as a system, including its trim state), but the principles can be outlined in general terms.

The process starts with the specification of the net system thrust $C_T = C_W$ and a requirement for an equal thrust sharing (i.e., $C_{T_u} = C_{T_l} = C_W/2$) between the two rotors. The loads on the upper rotor are determined from any initially presumed distribution of $\theta_u(r)$, and so giving a first solution to the distribution of $\lambda(r)$ on both rotors. A lift-curve slope, C_{l_α}, of 2π per radian can be assumed, although in any practical case C_{l_α} can be specified empirically (i.e., through a table lookup), or the linearized effects of compressibility on C_{l_α} can be accounted for using the Glauert correction if tabulated airfoil data are not available. Alternatively, both C_l and C_d can be specified directly in the BEMT by using airfoil tables. The thrust distribution per unit span dC_{T_u}/dr on the

upper rotor is then determined, and the net rotor thrust C_{T_u} is found by radial integration.

The goal of finding θ_u for a linear thrust distribution (i.e., $dC_{T_u}/dr = 2C_{T_u}$) was accomplished by means of a fixed-point iteration using Eq. (12) for a given trim state; the assumption of radial independence of each element in the BEMT allows θ_u to be determined section by section (rather than by using assumed spanwise shape functions), which as mentioned previously is an approach that has good validity except at the blade tips. During this process, the rotors were trimmed initially to carry equal thrust by adjusting the reference blade pitch angles by interation, and the resulting inflow and blade loading solutions then provide a good initial condition to proceed with the torque trim.

The inflow solution for the upper rotor then dictates its outflow velocities in the wake, and so defines the upstream flow velocity that is ingested into the lower rotor (assuming asymptotic wake contraction). The process of finding θ_l is then accomplished by numerically solving Eqs. (13) and (14), while imposing the same goal of a linear thrust distribution and uniform disk loading, i.e., $dC_{T_l}/dr = 2C_{T_l}$. This requirement produces uniform disk loading on the lower rotor, as well as uniform inflow distributions over the inner and outer regions of the rotor disk.

The process then continues by finding θ_u and θ_l by iteration to give a torque (power) balance on the two rotors (finding $|C_{Q_u} - C_{Q_l}| = 0$ to within a 0.05% error is sufficient) while relaxing the need for equal thrust sharing. The process converges smoothly and quickly, although at least 100 radial points over the blades must be used to define accurately the spanwise airloads over the two rotor disks less the spanwise loading gradients be inadequately resolved and the torque balance tolerance not be met. This discretization requirement poses some computational challenges for the FVM, and the differences in the discretizations used in the methods are one source of the differences seen in the results, as discussed previously.

Induced losses

A representative set of results for the optimal coaxial rotor are shown in Figs. 20–22. In this case, Harrington's rotor 2 (which has zero blade twist and no taper) was considered as the baseline, mainly because notable improvements in performance could be established relative to the known (measured) results in hovering flight. For the optimum rotor, it was designed to operate at a net system C_T of 0.008 at a torque balance.

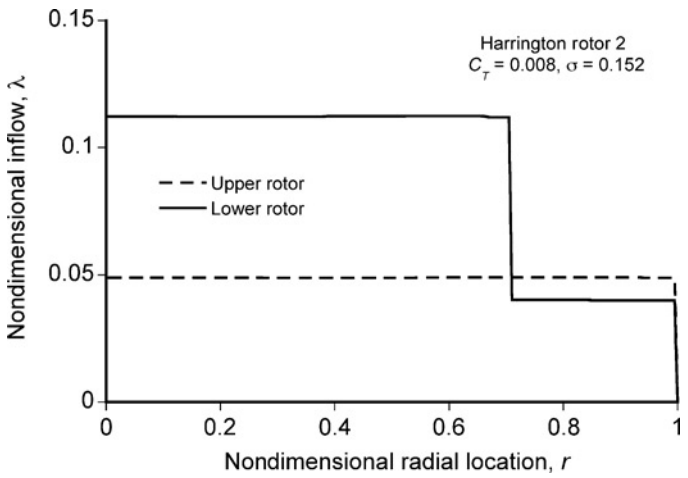

Fig. 20. Distribution of inflow on upper and lower rotors for an optimum coaxial rotor configuration. Harrington's rotor 2 was used as baseline (results obtained at a torque balance).

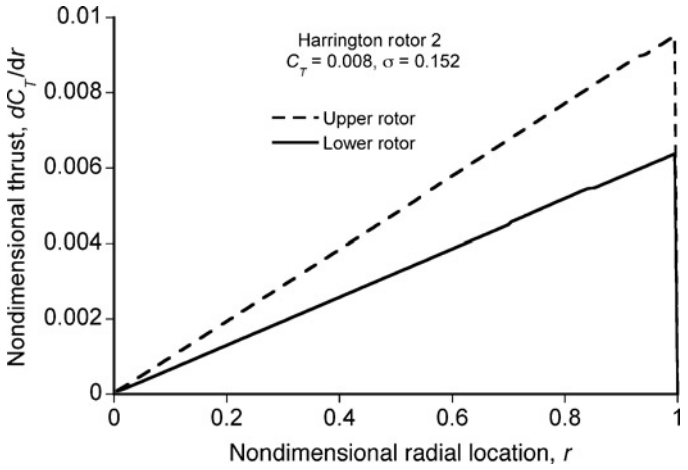

Fig. 21. Distribution of thrust on upper and lower rotors for an optimum coaxial rotor configuration. Harrington's rotor 2 was used as baseline (results obtained at a torque balance).

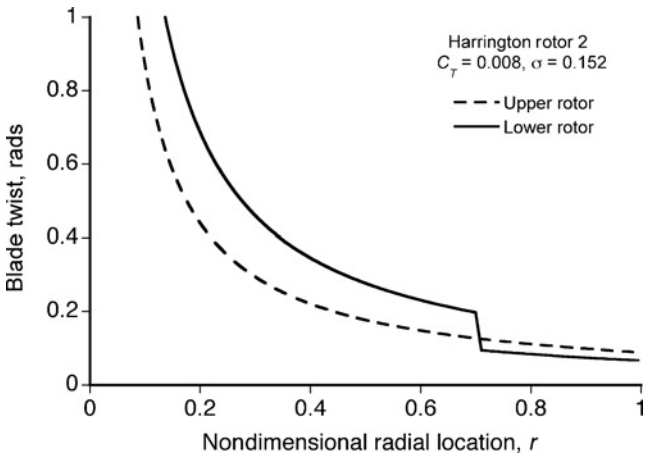

Fig. 22. Blade twist distribution required on the upper and lower rotors to produce ideal distributions of inflow. Harrington's rotor 2 was used as baseline (results obtained at a torque balance).

An ideal wake contraction of 70.7% (i.e., $A/A_r = 2$) from the upper rotor was assumed in this case, although as mentioned previously, the wake contraction may not be as large as this in practice.

Figure 20 shows the inflow distribution over the upper and lower rotors. Note that for each rotor the inflow is uniformly distributed, as required for uniform disk loading. Obviously, there is a much higher net inflow on the inboard part of the lower rotor, which of course is the signature produced by the slipstream from the upper rotor.

The linear thrust distribution shown in Fig. 21 confirms that uniform disk loading has indeed been achieved through the optimization of the blade twist. The need for a torque balance means now that there is a different thrust on the upper and lower rotors; the larger induced losses on the lower rotor means that a smaller thrust is required compared to that needed on the upper rotor to attain this torque balance. Recall that the load sharing depends on the net system thrust and trim state, so the blade design for optimal hovering performance is nonunique, although the form of the blade twist distribution will be geometrically similar in all cases (i.e., changed by a scaling factor).

The blade twist distribution (Fig. 22) to achieve uniform disk loading on each rotor is of particular interest. While a hyperbolic blade twist on

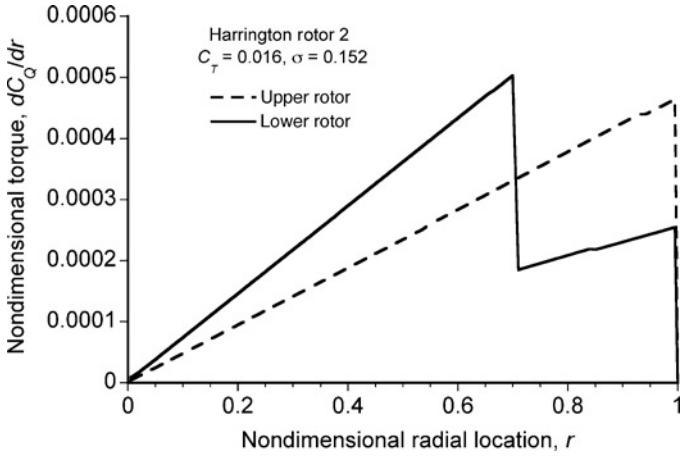

Fig. 23. Distribution of torque on upper and lower rotors for an optimum coaxial rotor configuration. Harrington's rotor 2 was used as baseline (results obtained at a torque balance).

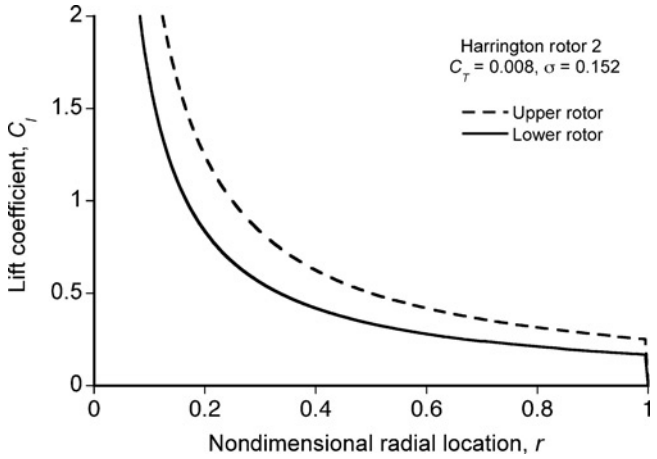

Fig. 24. Distribution of local lift coefficient on upper and lower rotors for an optimum coaxial rotor configuration. Harrington's rotor 2 was used as baseline (results obtained at a torque balance).

the upper rotor is an expected result, note that a double-valued form of hyperbolic twist is required on the lower rotor. This twist is needed to compensate for the outflow from the upper rotor so as to maintain the necessary uniform disk loading over the lower rotor. Clearly, the amount of blade twist required is considerable, but this is the twist needed to correct for the degraded lift that would otherwise be produced by the effects of the slipstream from the upper rotor. The blade pitch required to produce useful lift is only slightly larger than for the upper rotor, bearing in mind there is a torque balance on the coaxial as a system and that a higher average blade pitch angle is required on the upper rotor at this condition. Outside the slipstream boundary, it is obvious that the blade pitch requirements will be significantly reduced.

The torque distribution in Fig. 23 shows that the steeper gradients obtained on the inner part of the lower rotor from the slipstream of the upper rotor are offset on the outer part of the lower rotor. A torque balance was again specified in this case, so the net area under both torque curves is equal (i.e., $\int dC_{Q_u} = C_{Q_u} = \int dC_{Q_l} = C_{Q_l}$) to within the defined numerical convergence criteria.

Mean lift coefficients and profile losses

The corresponding distribution of local lift coefficients over the upper and lower rotors is shown in Fig. 24. As was apparent from the results in Fig. 21, the upper rotor of a coaxial generally carries a higher proportion of the total system thrust to achieve the necessary torque balance, therefore the upper rotor also operates at a higher average lift coefficient (about 0.504 in this particular case) than the lower rotor (about 0.338). This observation leads to two significant consequences.

First, the upper rotor operates at higher average blade section angles of attack, and so the blade operates at higher sectional lift coefficients and different lift-to-drag ratios compared to those on the lower rotor. To minimize profile losses, both rotors will need the blades to operate close to their best values of C_l/C_d, and this condition generally cannot be met precisely (assuming that both rotors have the same airfoil sections and tip Mach numbers) if they operate at different mean lift coefficients. While this difference is generally small (because the C_l/C_d curves of many airfoil sections are flat over a good range of angle of attack at their operational Mach numbers and Reynolds numbers), a true optimum coaxial rotor must still have all blade stations on both rotors operating as closely as possible to their best values of C_l/C_d. This goal will require hyperbolically tapered blades on both the upper and lower rotors, or a reasonable approximation to such a planform by using linear taper.

This blade planform design problem, however, will be more complicated for MAV designs, which have much more nonlinear blade section aerodynamics at their lower chord Reynolds numbers, and so reach their best sectional C_l/C_d values only at very specific operating conditions (i.e., at very specific angles of attack and Reynolds number). Nevertheless, the performance goals and blade design principles for full-scale and MAV-scale coaxial rotors are equivalent.

Second, for equal values of rotor solidity it is apparent that the upper rotor will dictate the stall margins of the rotor as a whole, and so the upper rotor may ultimately limit the net performance of the coaxial. One way to rectify this problem and to attain an optimum coaxial rotor is to increase the weighted solidity of the upper rotor and so reduce the average lift coefficients there and also decrease the weighted solidity of the lower rotor. While the practical construction of two rotors with different blade designs (both in terms of twist and solidity) will obviously be more expensive than one made using identical blade shapes throughout, this may be the price to pay for a coaxial rotor system that has the best overall efficiency with the largest performance and stall margins when in hover and/or in axial flight.

Again, the problem of optimizing the blade shapes of a coaxial rotor MAV is likely to be much more challenging because of the typically more nonlinear blade section characteristics and lower maximum lift coefficients that are found at lower chord Reynolds numbers (i.e., for those below 100,000). The ability to retain good stall margins in the overall rotor design also becomes more critical in this case.

Optimizing the harrington coaxial rotor

The hovering performance of the coaxial rotor with the optimally twisted blades (relative to the untwisted blades on the baseline Harrington rotor 2) is shown in Fig. 25 when using the BEMT. The corresponding values of the net induced power factor and *FM* are shown in Figs. 26 and 27, respectively.

The use of optimal blade twist (in this case for a design point at a net system $C_T = 0.008$, which is near maximum efficiency) gives a reduction in rotor power by lowering the induced losses. Note from Fig. 26 that for the baseline rotor the net induced power factor remains nominally constant and even slightly increases at higher thrusts. The optimum coaxial rotor shows a lower induced power factor at the design

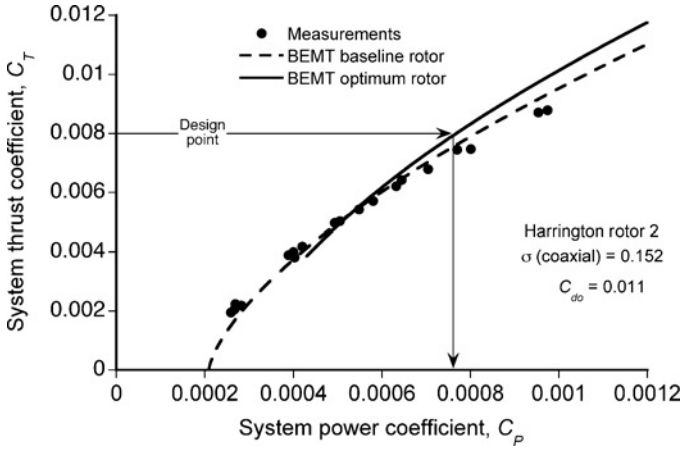

Fig. 25. Performance polar of the optimal coaxial rotor relative to the baseline Harrington rotor 2 (results obtained at a torque balance).

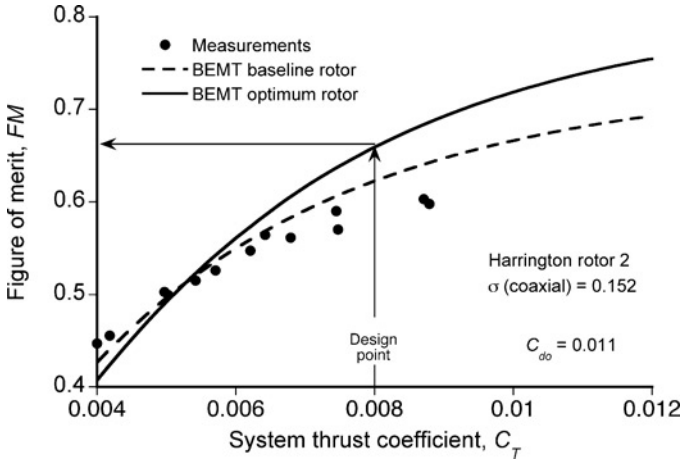

Fig. 27. Figure of merit of the optimal coaxial rotor relative to the baseline Harrington rotor 2 (results obtained at a torque balance).

point, and this factor decreases only slightly at higher thrusts. About a 9% increase in *FM* is obtained from the use of blade twist, and another benefit is that better values of *FM* are obtained at higher values of C_T. This *FM* would be further increased if the radial wake contraction from the upper rotor turned out to be smaller than 0.82, i.e., representing a rotor spacing effect, as discussed previously.

The results in Fig. 24 suggest that profile losses can be minimized by using hyperbolic blade taper, which will be of the form $\sigma_u = \sigma_{u_{\text{tip}}}/r$ and $\sigma_l = \sigma_{l_{\text{tip}}}/r$. In this case, the leading part of the overall profile power (assuming constant profile $C_d = C_{d_0}$) will be reduced to $C_{P_0} = 2\sigma C_{d_0}/9$ compared to $C_{P_0} = 2\sigma C_{d_0}/8$ with rectangular blades for the combination of the upper and lower rotors, and so elevating the *FM* by a further 3%–5%, depending on the actual operating state of the rotor. In practice, linear taper along the blade will probably accomplish much of the desired performance improvements, as it does for a single rotor.

Clearly, the potential overall performance gains with a coaxial rotor through blade shape optimization can be significant, i.e., nearly a 15% increase in efficiency is possible relative to an unoptimized design. Nevertheless, because the primary losses in a coaxial rotor system in hover stem from rotor-on-rotor interference, the induced losses cannot be reduced (even through an aggressive optimum blade design) any further than the lowest bounds as given by the SMT (depending on thrust sharing and overall operating conditions). However, the use of something close to the required double hyperbolic form on the lower rotor will help significantly in extracting maximum aerodynamic efficiency from any type of coaxial rotor system.

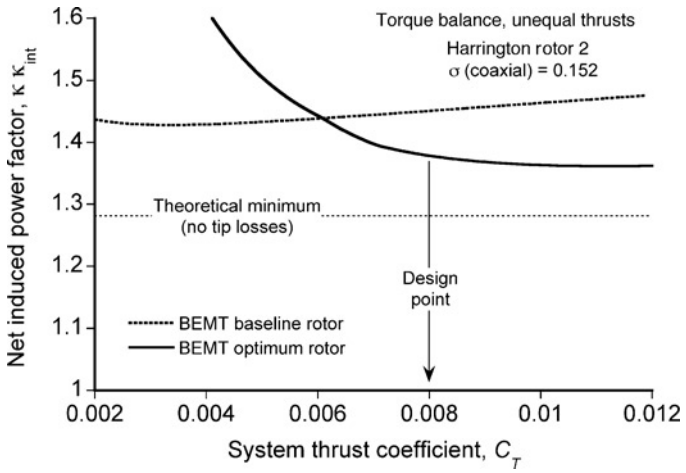

Fig. 26. Induced power factor of the optimal coaxial rotor relative to the baseline Harrington rotor 2 (results obtained at a torque balance).

Conclusions

A blade-element momentum theory for a coaxial rotor that operates in hover and axial flight was established. The primary motivation for the work was develop a relatively parsimonious theory (and as free as possible from empirical inputs) to help provide the best possible starting point for the formal optimization of a coaxial rotor system that may have to operate under a variety of design, operational, and other constraints, including low Reynolds number flight. The theory was validated with performance measurements of coaxial helicopter rotors that operated in hover, and with measurements for contrarotating coaxial propellers operating in axial forward flight, all at higher blade chord Reynolds numbers. The following conclusions have be drawn from this work:

1) The BEMT was found to agree well with measured coaxial rotor performance. Predictions in hovering flight correlated well with the classic measurements of Harrington. In axial flight, coaxial contrarotating propeller performance measurements helped to validate the BEMT, with reasonably good success over a wide range of operating conditions. The predictions of spanwise loads from the BEMT were also validated against results from a free-vortex wake analysis, thereby giving confidence in the overall predictive capabilities of the BEMT when used to model coaxial rotor systems.

2) It was shown that the optimum condition for minimum induced losses on a coaxial rotor operated in hover occurs when both the upper and lower rotors operate with uniform disk loadings and at a balanced torque. This operating condition corresponds to linear distributions of thrust over the blades of both the upper and lower rotors. The ideal case also corresponds to uniform inflow on the upper rotor, but a double-valued uniform inflow on the lower rotor. In this case, the optimum blade twist for the lower rotor was shown to have a double hyperbolic form, with the break point in the blade twist being at the location where the outer part of the wake boundary from the upper rotor was assumed to impinge on the lower rotor.

3) The sensitivity of coaxial rotor performance to the assumed wake contraction from the upper rotor was explored, i.e., a parameter that reflects the effects of rotor plane separation. The results showed that the combined induced losses were relatively insensitive to the wake contraction over the expected practical range of rotor separations that might be used on a helicopter. This result, however, may not apply as universally to a coaxial propeller or proprotor. In the limiting case where the upper and lower rotors become coplanar, the equations of the BEMT must be modified so that both rotors will share the same distributions of induced velocities, and the induced losses are highest in this case.

4) The BEMT was used to design an optimum hovering coaxial rotor to achieve minimum losses and a maximum figure of merit. A double hyperbolic blade twist distribution on the lower rotor is needed in this case. This twist was shown to improve the figure of merit over a baseline rotor system by up to about 10%. The ability to improve further upon the figure of merit is limited by the persistence of rotor-on-rotor interference losses in all axial flight operating conditions.

5) A by-product of the coaxial rotor optimization showed that the upper and lower rotors operated at different thrust and mean lift coefficients. This suggests that separate optimization of the blade planforms on both of the rotors will be required to produce distributions of lift coefficients over the blades that can minimize profile losses by having all the blade sections on both rotors work close to their best lift-to-drag ratios. This effort will be especially important to maintain the propulsive efficiency of a coaxial proprotor in forward flight.

Acknowledgments

This work has been partly supported by the Army Aviation Applied Technology Directorate (AATD) and by the Office of Naval Research (ONR). The authors are grateful to their many professional colleagues for their advice and suggestions during this study. In particular, the additional contributions of Monica Syal to this work are appreciated. Franklin Harris has kindly provided the converted and tabulated digitized data from the Evans and Liner high-speed propeller tests. Finally, the comments and suggestions of the three anonymous reviewers of this paper are gratefully acknowledged. Note that any opinions, findings, conclusions, or recommendations expressed in this paper are those of the authors and do not necessarily reflect the views of the University of Maryland, the sponsoring agencies, or any other organization or persons with which the authors may have been associated.

References

[1]Bagai, A., "Aerodynamic Design of the X2 Technology Demonstrator Main Rotor Blade," American Helicopter Society 64th Annual Forum Proceedings, Montréal, Canada, April 28–May 1, 2008.

[2]Preator, R., Leishman, J. G., and Baldwin, G. D., "Performance and Trade Studies of Mono Tiltrotor Design," American Helicopter Society 61st Annual Forum Proceedings, Grapevine, TX, June 1–3, 2005.

[3]Pines, D. J., and Bohorquez, F., "Challenges Facing Future Micro-Air-Vehicle Development, *Journal of Aircraft*, Vol. 43, (2), March–April 2006, pp. 290–305.

[4]Playle, S. C., Korkan, K. D., and von Lavante, E., "A Numerical Method for the Design and Analysis of Counter-Rotating Propellers," *Journal of Propulsion and Power*, Vol. 2, (1), January–February 1986, pp. 57–63.

[5]Coleman, C. P., "A Survey of Theoretical and Experimental Coaxial Rotor Aerodynamic Research," 19th European Rotorcraft Forum Proceedings, Cernobbio, Italy, September 14–16, 1993.

[6]McAlister, K. W., Tung. C., Wilson, J. S., and Rand, O., "Experimental and Numerical Study of a Model Coaxial Rotor," American Helicopter Society 62nd Annual Forum Proceedings, Phoenix, AZ, May 9–11, 2006.

[7]McAlister, K. W., and Tung. C., "Experimental Study of a Hovering Coaxial Rotor with Highly Twisted Blades," American Helicopter Society 64th Annual Forum Proceedings, Montréal, Canada, April 29–May 1, 2008.

[8]Andrew, M. J., "Coaxial Rotor Aerodynamics in Hover," *Vertica*, Vol. 5, 1981, pp. 163–172.

[9]Saito, S., and Azuma, S., "A Numerical Approach to Coaxial Rotor Aerodynamics," Seventh European Rotorcraft and Powered Lift Aircraft Forum, Garmisch–Partenkirchen, Federal Republic of Germany, September 8–11, 1981.

[10]Zimmer, H., "The Aerodynamic Calculation of Counter Rotating Coaxial Rotors," Eleventh European Rotorcraft Forum, London, September 10–13, 1985.

[11]Valkov, T., "Aerodynamic Loads Computation on Coaxial Hingeless Helicopter Rotors," Paper AIAA 90-0070, 28th Aerospace Sciences Meeting, Reno, NV, January 8–11, 1990.

[12]Kim, H. W., and Brown, R. E., "Coaxial Rotor Performance and Wake Dynamics in Steady and Manoeuvring Flight," American Helicopter Society 62nd Annual Forum Proceedings, Phoenix, AZ, May 9–11, 2006.

[13]Lakshminarayan, V. K., and Baeder, J. D., "Computational Investigation of Coaxial Rotor Aerodynamics in Hover," American Helicopter Society Specialist's Conference Proceedings on Aeromechanics, San Francisco, CA, January 23–25, 2008.

[14]Weick, F. E., *Aircraft Propeller Design*, McGraw-Hill Book Co., Inc., New York, NY, 1930.

[15]Froude, W., "On the Elementary Relation between Pitch, Slip and Propulsive Efficiency," *Transactions of the Institute of Naval Architects*, 19, 1878, pp. 47–57.

[16]Drzewiecki, S, *Théorie Générale de l'Hélice Propulsive*, Gauthier–Villars, Paris, 1920.

[17]Tokaty, G. A., *A History and Philosophy of Fluid Mechanics*, Foulis & Co., Henley-on-Thames, UK, 1971.

[18]Gessow, A., "Effect of Rotor-Blade Twist and Plan-Form Taper on Helicopter Hovering Performance," NACA Technical Note 1542, 1948.

[19]Gessow, A., and Myers, G. C., *Aerodynamics of the Helicopter*, MacMillan Co., New York, NY, 1952, pp. 73–75.

[20]Leishman, J. G., *Principles of Helicopter Aerodynamics*, 2nd edition, Cambridge University Press, New York, NY, 2006.

[21]Lock, C. N. H., Bateman, H., and Townend, H. C. H., "Experiments to Verify the Independence of the Elements of an Airscrew Blade," British ARC R & M 953, 1924.

[22]Leishman, J. G., and Ananthan, S., "Aerodynamic Optimization of a Coaxial Proprotor," American Helicopter Society 62nd Annual Forum Proceedings, Phoenix, AZ, May 9–11, 2006.

[23]Leishman, J. G., and Syal, M., "Figure of Merit Definition for Coaxial Rotors," *Journal of the American Helicopter Society*, Vol. 53, (3), July 2008, pp. 290–300.

[24]Taylor, M. K., "A Balsa-Dust Technique for Air-Flow Visualization and Its Application to Flow through Model Helicopter Rotors in Static Thrust," NACA Technical Note 2220, 1950.

[25]Lock, C. N. H., "Interference Velocity for a Close Pair of Contra-Rotating Airscrews," British R&M No. 2084, July 1941.

[26]Davidson, R. E., "Optimization and Performance Calculation of Dual-Rotation Propellers," NASA TP 1948, December 1981.

[27]Johnson, W., *Helicopter Theory*, Princeton University Press, Princeton, NJ, 1980.

[28]Leishman, J. G., Bhagwat, M. J., and Bagai, A., "Free-Vortex Filament Methods for the Analysis of Helicopter Rotor Wakes," *Journal of Aircraft*, Vol. 39, (5), September–October, 2002, pp. 759–775.

[29]Harrington, R. D., "Full-Scale Tunnel Investigation of the Static Thrust Performance of a Coaxial Helicopter Rotor," NACA Technical Note 2318, 1951.

[30]Payne, P. R., *Helicopter Dynamics and Aerodynamics*, Pitman & Sons, London, 1959.

[31]Bagai, A., and Leishman, J. G., "Free-Wake Analysis of Tandem, Tilt-Rotor and Coaxial Rotor Configurations," *Journal of the American Helicopter Society*, Vol. 41, (3), 1996, pp. 196–207.

[32]Bhagwat, M. J., and Leishman, J. G., "Stability, Consistency and Convergence of Time-Marching Free-Vortex Rotor Wake Algorithms," *Journal of the American Helicopter Society*, Vol. 46, (1), January 2001, pp. 59–71.

[33]Platt, R. J., "Thrust Loading of the NACA 3-(3)(05)-05 Eight-Blade Dual-Rotating Propeller as Determined from Wake Surveys," NACA Research Memorandum RM L52103 (unclassified), October 1932.

[34]Evans, A. J., and Liner, G., "Wind Tunnel Investigation of the Aerodynamic Characteristics of a Full-Scale Supersonic-Type Three-Blade Propeller at Mach Numbers to 0.96," NACA Report 1375, May 1958.

[35]Biermann, D., and Hartman, E., "Wind-Tunnel Tests of Four- and Six-Bladed Single- and Dual Rotating Tractor Propellers," NACA Report 747, July 1940.

[36]Naiman, I., "Method of Calculating Dual-Rotating Propellers from Airfoil Characteristics," NACA Wartime Report, ARR No. 3E24 (unclassified), May 1943.